AIP | Applied Physics Letters

Magnetic field control and wavelength tunability of SPP excitations using Al2O3/SiO2/Fe structures

Terunori Kaihara, Hiromasa Shimizu, Alfonso Cebollada, and Gaspar Armelles

Citation: Applied Physics Letters **109**, 111102 (2016); doi: 10.1063/1.4962653
View online: http://dx.doi.org/10.1063/1.4962653
View Table of Contents: http://scitation.aip.org/content/aip/journal/apl/109/11?ver=pdfcov
Published by the AIP Publishing

Magnetic field control and wavelength tunability of SPP excitations using $Al_2O_3/SiO_2/Fe$ structures

Terunori Kaihara,[1] Hiromasa Shimizu,[1,a)] Alfonso Cebollada,[2] and Gaspar Armelles[2]
[1]*Department of Electrical and Information Engineering, Tokyo University of Agriculture and Technology, 2-24-16 Naka-cho, Koganei, Tokyo 184-8588, Japan*
[2]*IMM-Instituto de Microelectrónica de Madrid (CNM-CSIC), Isaac Newton 8, PTM, E-28760 Tres Cantos, Madrid, Spain*

(Received 7 June 2016; accepted 29 August 2016; published online 13 September 2016)

Here, we show the high wavelength tunability and magnetic field modulation of surface plasmon polaritons (SPPs) of a waveguide mode that Double-layer Dielectrics and Ferromagnetic Metal, $Al_2O_3/SiO_2/Fe$, trilayer structures exhibit when excited in the Otto configuration of attenuated total reflection setup. First by modeling, and then experimentally, we demonstrate that it is possible to tune the wavelength at which the angular dependent reflectance of these structures reaches its absolute minimum by simply adjusting the SiO_2 intermediate dielectric layer thickness. This precise wavelength corresponds to the cut-off condition of SPPs' waveguide mode supported by the proposed structure, and it can be then switched between two values upon magnetization reversal of the Fe layer. In this specific situation, a large enhancement of the transverse magneto-optical effect is also obtained. *Published by AIP Publishing.* [http://dx.doi.org/10.1063/1.4962653]

Surface plasmon polaritons (SPPs) are quasi-particles generated from the coupling between an electromagnetic (EM) wave and the collective oscillations of a free electron gas at the interface of two media with permittivities of opposite signs, such as a metal and a dielectric. It has been shown that SPPs play an important role in systems presenting magneto-optical (MO) activity and plasmon resonances.[1] In particular, linked to the resonance enhancement of the electromagnetic (EM) field in the MO active component,[2] large increases in the MO activity have been found in magnetoplasmonic systems in the form of nano-particle,[3,4] nanodisk,[5–7] nano-ring,[8,9] continuous/processed multilayered films,[10–12] and so on. On the other hand, the MO effect provides SPPs with the magnetic field modulation of the propagation constants,[13–15] or the propagation losses[14,16,17] of SPPs in complex continuous film structures with ferromagnetic components. These characteristics are potentially feasible for a wide range of applications, including chemical/biological sensors,[18] magnetically controllable modulators and interferometers,[13] and optical isolators and circulators[14–17] compatible with Photonic Integrated Circuits (PIC). Conventionally, a magneto-optic garnet is used for free-space fiber-optics nonreciprocal devices, such as optical isolators and circulators because of its large MO effect and low optical absorption. When it comes to integrated photonics, however, integration of MO garnets with optical waveguide platforms made of III–V compound semiconductors, silicon, and silica is challenging because of the large mismatching in physical properties. For example, the lattice constant of yttrium iron garnet $Y_3Fe_5O_{12}$ (YIG) is 1.238 nm, whereas that of silicon is 0.543 nm, and the linear thermal expansion coefficients of YIG is 10.4×10^{-6} while that of silicon $2.33 \times 10^{-6}\ K^{-1}$.[19] The advantages of metallic MO systems with SPPs over the MO garnets are the compatibility of metals with these PIC platforms and conventional CMOS processes, more than a hundred times larger MO constant of ferromagnetic metals in off-diagonal permittivity than that of MO garnets even without being a single crystal, and a contribution of the highly confined EM field distribution by SPPs to device downsizing and the enhancement of the MO effect. All these features are suitable for ongoing miniaturization-oriented industries.

Up to now, most of the experimental studies to explore the effect that a magnetic field has on the properties of propagating plasmons have been carried out exciting SPPs with a grating or in an attenuated total reflection (ATR) setup in Kretschmann-Raether (K-R) configuration.[20] In this configuration, surface plasmons are excited in metallic layers deposited on dielectric prisms by illumination through the prism, and the optimum coupling between the incident photon and the SPP mode is determined by the thickness of the metal layer. On the other hand, if an Otto configuration[21] is used instead (by the insertion of a dielectric layer of lower refractive index between the prism and the metallic layer), an additional degree of tunability is available, since the coupling between the photon and the SPP mode can be further optimized by the thickness of the intermediate layer between the prism and the metal layer. In fact, a Double-layer Dielectrics and Ferromagnetic Metal (DDFM) structure,[16,17,22,23] which is equivalent to an Otto configuration, has been recently proposed due to its expected superior performance applicable for optical isolators and, in general, nonreciprocal devices. In this model structure, by stacking up films of a ferromagnetic metal and two dielectric layers of low and high refractive indices, it is possible to control the confinement of SPPs achieving low propagation losses with a large MO figure of merit at the cut-off condition of the waveguide mode. Even though the long SPP propagation on the DDFM waveguide has recently been reported,[22] the experimental realization to

a)Author to whom correspondence should be addressed. Electronic mail: h-shmz@cc.tuat.ac.jp

exactly obtain the cut-off condition is challenging due to the fabrication accuracy (error roughly within ~10 nm) particularly in a minute waveguide structure, and as a consequence, there are no experimental reports on the actual magnetic modulation and MO response in this kind of systems. From the technical point of view, if these structures are illuminated using a prism in attenuated total reflection (ATR) setup in an Otto configuration fashion, the optimum excitation condition can be found as the smallest reflection dip, which in turn corresponds to the excitation of the waveguide mode at the cut-off condition[23] and will depend on the magnetization of the ferromagnetic layer.

Therefore, the purpose of this work is to design and fabricate such DDFM structures capable of supporting waveguide modes just at the cut-off condition and subsequently study their SPP magnetic modulation capabilities. This will be done by exploring how the reflection dip depends on the device film thickness, wavelength relevant for telecom applications, and magnetization with the Otto configuration of the ATR setup. The strong enhancement and tunability of the MO activity obtained in this configuration will be also presented.

The structure used consists of a SiO_2/Fe bilayer deposited on top of an Al_2O_3 substrate. If the structure is illuminated from the high refractive index layer (Al_2O_3), there is an angle of incidence at which the incoming wave turns into an evanescent wave inside the low refractive index layer (SiO_2) and couples with SPPs at the Fe interface (Fig. 1(a)).

Given that SPPs propagate in the z-direction and a magnetic field enough for magnetization saturation is applied perpendicular to the incident plane along the y-axis (Fig. 1(a)), a ferromagnetic metal Fe has the relative permittivity tensor,

$$\tilde{\varepsilon}_r = \begin{pmatrix} \varepsilon_r & 0 & \varepsilon_{\mathrm{MO}} \\ 0 & \varepsilon_r & 0 \\ -\varepsilon_{\mathrm{MO}} & 0 & \varepsilon_r \end{pmatrix}, \qquad (1)$$

where ε_r is the relative permittivity without magnetization and $\varepsilon_{\mathrm{MO}}$ represents the MO constant. Assuming Eq. (1) in a matrix method and Effective index theory,[24] we calculated the reflectance of p-polarized light (R_{pp}) and a waveguide mode in this structure. When the low refractive index layer (SiO_2) is very thick, the SPP of a waveguide mode is confined at the interface between the Fe and the SiO_2. When the SiO_2 layer narrows down, there is a specific thickness at which the SPP is pulled off from the Fe/SiO_2 interface to the high refractive index layer (Al_2O_3) and is no longer confined as a waveguide mode. This condition is defined as the cut-off.[16,17] In this work, we found that this cut-off depends not only on the thickness of the low refractive index layer but also on the wavelength. Figure 1(b) shows a SPP field profile (magnetic field, $|\boldsymbol{H}|^2$) at a thickness of the SiO_2 layer of $t = 586$ nm, where the cut-off condition occurs at a wavelength of $\lambda = 1.3\,\mu$m. With increasing the wavelength, the effective thickness of the SiO_2 becomes thinner for the SPP to be a waveguide mode, and the mode leaks out to the Al_2O_3 layer leading to an unguided mode whereas the opposite occurs for shorter wavelengths as shown in Fig. 1(b). In ATR configuration, the SPP resonance is associated with the momentum matching condition with the incident light as

$$k_{spp} = \frac{2\pi}{\lambda} n_{inc} \sin(\theta_{inc}), \qquad (2)$$

where k_{spp} is the wavenumber of the SPPs, n_{inc} is the refractive index of a medium where the light comes from (the Al_2O_3layer in our case), and θ_{inc} is the angle of incidence. In fact, the k_{spp} is a complex number while $(2\pi/\lambda)\, n_{inc} \sin(\theta_{inc})$ is a real number; therefore, Eq. (2) is not perfectly satisfied at any angle of incidence. However, at the cut-off condition given by the optimized wavelength or thickness of the low-index layer (SiO_2), the propagation loss of the SPPs nearly disappears, meaning that the k_{spp} becomes real number possible to fulfill Eq. (2) at a certain angle of incidence. Our previous study[23] shows that the reflectance, R_{pp}, can be minimized at the cut-off because perfect momentum matching occurs, and the energy of the light is most effectively transmitted to the SPPs, and least comes back. Figures 2(a) and 2(b) show, for the case presented in Fig. 1(b), ATR-like curves for R_{pp} as functions of angle of incidence and the wavelength, respectively.

Although the plasmonic resonance for a ferromagnetic metal is not as sharp as noble metals show, the reduction of R_{pp} is significant at the cut-off condition at $\lambda = 1.3\,\mu$m and $\theta_{inc} = 54.5°$. In order to tune the wavelength where the cut-off occurs by optimizing the thickness of the low-index SiO_2 layer, we first found the cut-off of the waveguide mode by changing the thickness of the SiO_2 at the arbitrarily designed wavelength based on the Effective index theory; the critical thickness where the waveguide mode is no longer found renders the cut-off condition.[16,17] When a magnetic field is applied perpendicular to the plane of incidence, the MO activity of the Fe layer induces a modulation of SPP wave vector, and thus the cut-off condition can be changed by switching the direction of magnetization of the Fe layer. If we design the SiO_2 thickness as $t = 586$ nm and 760 nm, the minimum reflectance of R_{pp} would appear around the popular optical telecommunication wavelength of $\lambda = 1.3\,\mu$m and 1.55 μm, respectively, as shown in Fig. 2(c). Note that to emphasize the reflectance minimum at the cut-off, we show the reflectance in a logarithmic scale. In Fig. 2(d), we plot the relationship between the wavelength and the SiO_2 thickness where the cut-off occurs for opposite magnetic saturations ±M of the Fe layer.

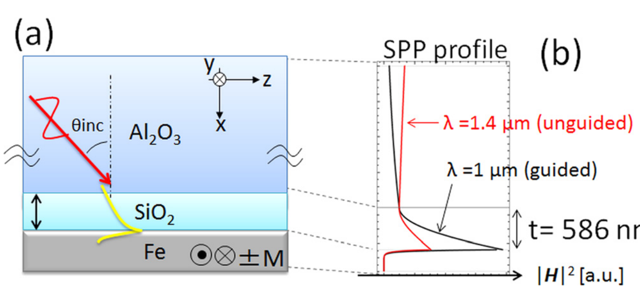

FIG. 1. (a) A trilayer structure consisting of Al_2O_3/SiO_2/Fe. The tilted red arrow represents the incident light while the yellow curve the distribution of the SPP. (b) The SPP field profile ($|H|^2$) at $\lambda = 1\,\mu$m (black curve) and 1.4 μm (red curve) for the thickness of the SiO_2 layer, $t = 586$ nm.

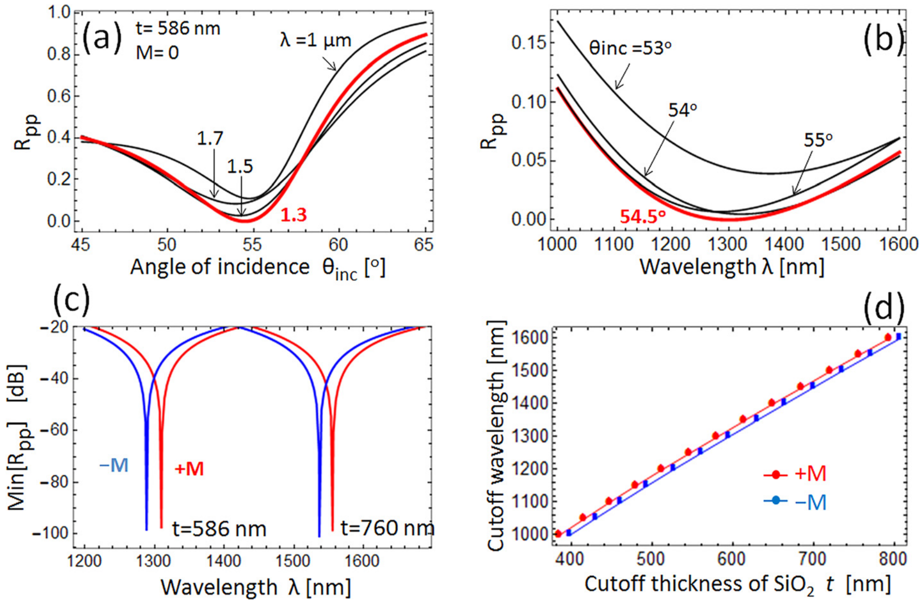

FIG. 2. The calculated reflectance of R_{pp} as a function of the angle of incidence (a) and wavelength (b) at $t = 586$ nm without magnetization. (c) The wavelength dependence of the reflectance minimum of p-polarized light, Min[R_{pp}], for $t = 586$ nm and 760 nm. (d) The relationship between the wavelength and the thickness of the SiO_2 layer, where the cut-off condition occurs. The red and blue curves in graphs represent the positive (+M) and negative (–M) magnetizations, respectively.

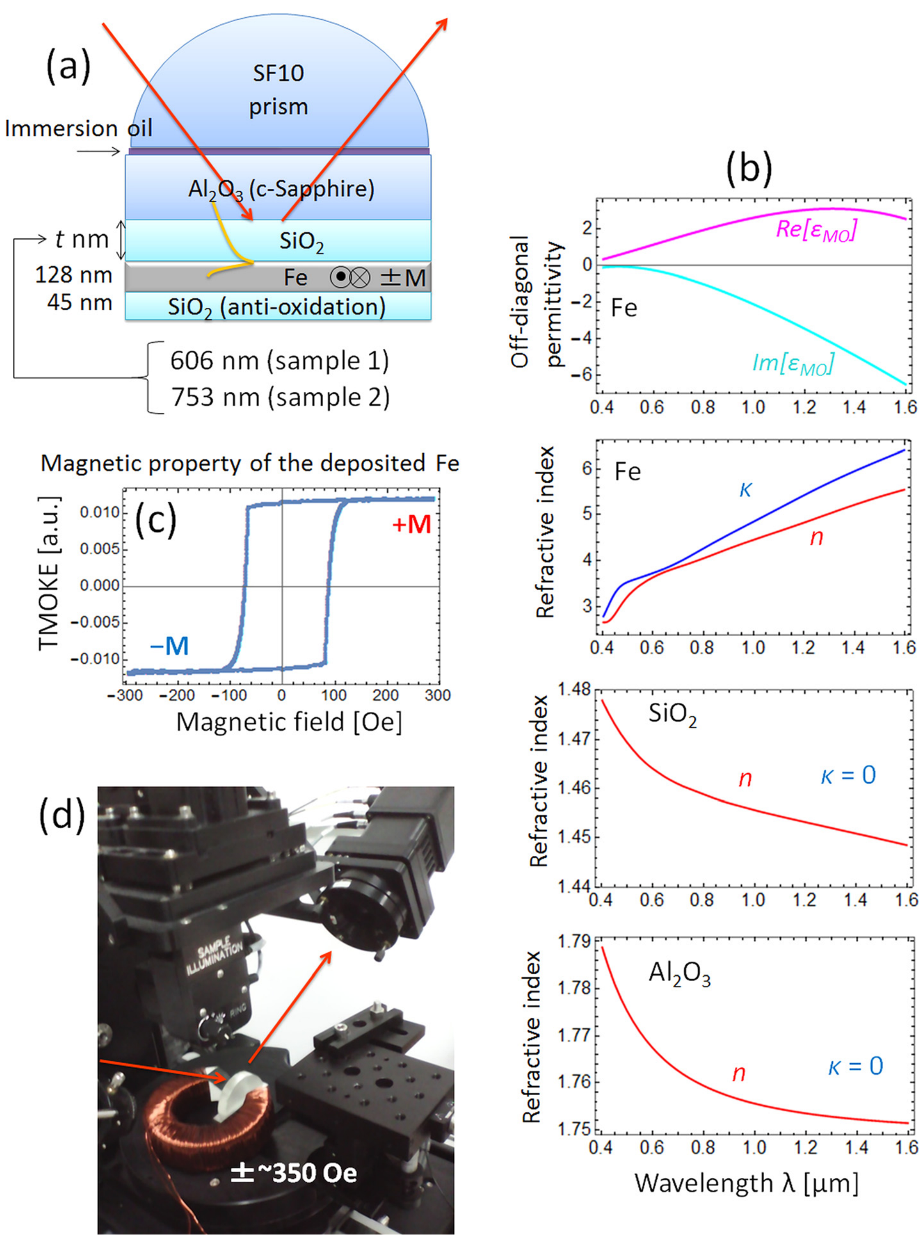

FIG. 3. (a) A schematic diagram of the fabricated Al_2O_3/SiO_2 ($t = 606$ nm (sample 1) or 753 nm (sample 2))/Fe structure. An SF10 prism is mounted on top of the substrate for the ATR experiment. (b) Experimentally obtained off-diagonal complex relative permittivity of the Fe layer (ε_{MO}), and the real (n) and imaginary (κ) parts of refractive indices of the Fe, SiO_2, and Al_2O_3 layers as a function of the wavelength. (c) The external magnetic field dependence of the transverse MO effect (hysteresis loop of TMOKE) of the deposited Fe measured via reflection. (d) A picture of the experimental setup using a spectroscopic ellipsometer and an electromagnet in the Voigt geometry. The red arrows represent the ray of light.

After carrying out this theoretical analysis, we prepared two samples aimed at the optical telecommunication wavelengths, around $\lambda = 1.3\,\mu$m and $1.55\,\mu$m, to demonstrate the flexible tunability of our method by the following process. The arbitrary SiO_2 layer (t nm) and the thick Fe layer (128 nm) were consecutively deposited by electron beam evaporation and sputtering on a c-sapphire (Al_2O_3) substrate, respectively. A SiO_2 cap layer (45 nm) was subsequently deposited on the Fe layer for anti-oxidation. The thickness of the samples was confirmed by using X-ray reflectivity (XRR) and spectroscopic ellipsometry, which were Al_2O_3/SiO_2 ($t = 606$ nm)/Fe/SiO_2 (sample 1) and Al_2O_3/SiO_2 ($t = 753$ nm)/Fe/SiO_2 (sample 2) as shown in Fig. 3(a). The optical constants of the samples were determined by spectroscopic ellipsometry including the off-diagonal elements of the permittivity tensor of Fe based on the magneto-optical ellipsometry technique (Fig. 3(b)).[25–27] We also characterized the magnetic property of the deposited Fe by measuring a magnetic hysteresis loop of transverse MO effect (TMOKE) from the backside of the sample, isolating the Fe from the DDFM system. The Fe showed an in-plane saturation magnetic field of $\sim$200 Oe (Fig. 3(c)). According to the hysteresis loop of the TMOKE, the magnetic field dependence of the MO signal of our Fe layer is a square loop, and thus the shift of the measured values by changing a magnetic field will have only two discrete points such as the calculated red (+M) and blue (–M) curves in Fig. 2(c).

For the ATR experiment, an SF10 semi-circular prism was attached to the Al_2O_3 substrate by a refractive index matching oil as schematically depicted in Fig. 3(a). The measurements were done using a Woollam ellipsometer model M-2000 equipped with a high-speed CCD array which allows us to collect the entire spectrum in a few seconds, while applying an external magnetic field of $\pm$350 Oe in the Voight geometry with changing the wavelength from 400 nm to 1688.5 nm and the angle of incidence from 45° to 70° (Fig. 3(d)).

Figures 4(a) and 4(b), respectively, show the reflectance, $R_{pp}/R_{ss}(\pm\mathrm{M})$, curves for samples 1 and 2 as a function of the angle of incidence at wavelengths for the cut-off and distant from the cut-off condition. We plot every minimum value of the $R_{pp}/R_{ss}(\pm\mathrm{M})$ as a function of the wavelength in Figs. 4(c) and 4(d). The absolute minimum reflectance for the positive magnetization in sample 1 is found at $\lambda = 1338.0$ nm and $\theta_{inc} = 55.4°$ while for the negative magnetization $\lambda = 1317.5$ nm and $\theta_{inc} = 55.3°$ (Figs. 4(a) and 4(c)). On the other hand, those in sample 2 are found at $\lambda = 1546.6$ nm and $\theta_{inc} = 54.1°$ for the positive magnetization (Figs. 4(b) and 4(d)) while at $\lambda = 1529.4$ nm and $\theta_{inc} = 54°$ for the negative magnetization. The agreement between the calculated (designed) and the experimental curves in Figs. 4(c) and 4(d) is remarkable, demonstrating the high tunability of the cut-off wavelength by adjusting the SiO_2 layer thickness and its

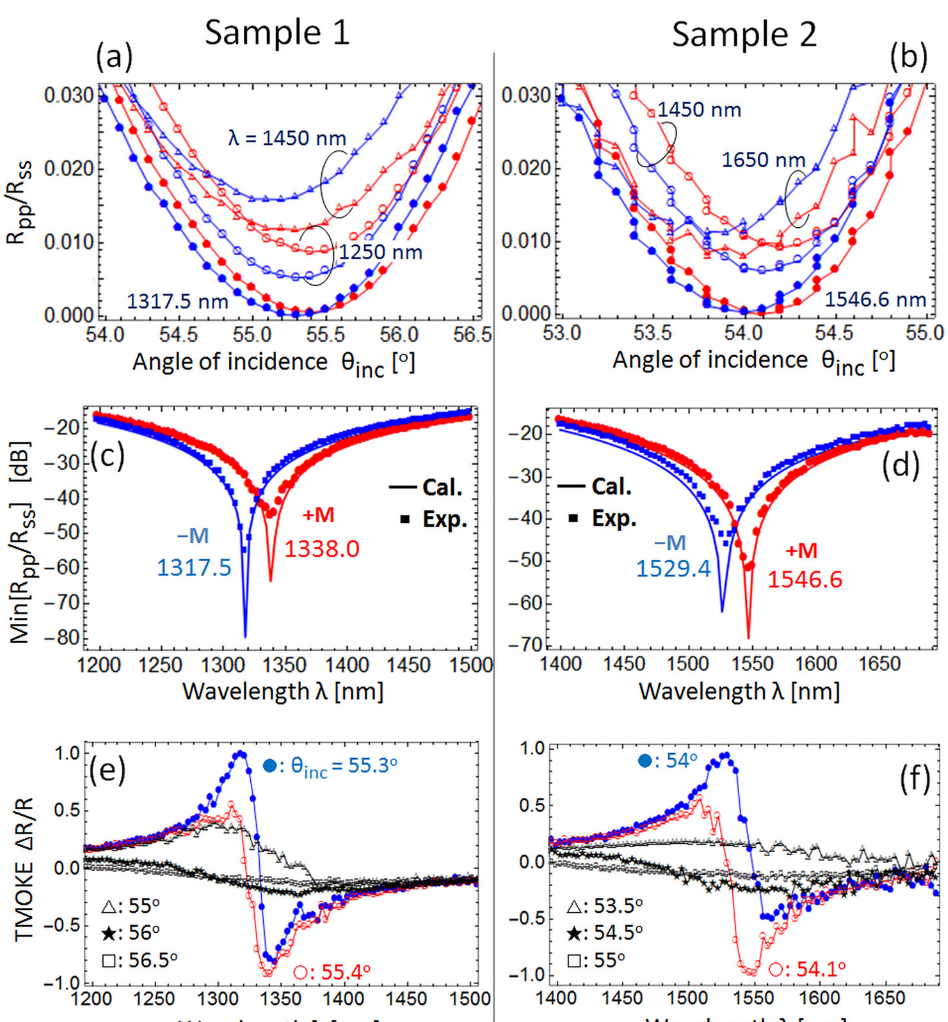

FIG. 4. (a) and (b) Reflectance, R_{pp}/R_{ss}, of samples 1 and 2 (same vertically hereafter) as a function of the angle of incidence for positive (red curves) and negative (blue curves) magnetizations. (c) and (d) The reflectance minimum, Min[R_{pp}/R_{ss}], for each individual wavelength. The solid curves represent calculations while the dots are experimental results. The numbers written in the graphs show the wavelength for which the experimental minimum is obtained. (e), (f) TMOKE intensity, $\Delta R/R$, as a function of wavelength at the fixed angles of incidence written in the graphs.

modulation upon magnetization reversal. Note that the calculated curves were obtained at the same discrete points where the measurement was done. The drops at the cut-off in the experimental curves were obscured somewhat by the surface roughness of the layers and/or the prism and a noise level of our measurement system. Figures 4(e) and 4(f) show $(R_{pp}/R_{ss}(+\mathrm{M}) - R_{pp}/R_{ss}(-\mathrm{M}))/(R_{pp}/R_{ss}(+\mathrm{M}) + R_{pp}/R_{ss}(-\mathrm{M}))$, which is equivalent to a TMOKE intensity defined as

$$\frac{\Delta R}{R} = \frac{R_{pp}(+M) - R_{pp}(-M)}{R_{pp}(+M) + R_{pp}(-M)}, \tag{3}$$

as a function of the wavelength for fixed angles of incidence. In Fig. 4(e), the $\theta_{inc} = 55.3°$ and $55.4°$ have much larger TMOKE intensity than the other angles do. These two angles are very close and thus show similar curves; however, the maximum values for the $\theta_{inc} = 55.3°$ and $55.4°$ are found at different wavelengths of $\lambda = 1317.5\,\mathrm{nm}$ and $1338.0\,\mathrm{nm}$, respectively. Note that these angles and wavelengths correspond to where the reflectance minima are found as shown in Figs. 4(a) and 4(c). Similarly, the $\theta_{inc} = 54°$ and $54.1°$ in Fig. 4(f), respectively, correspond to the minima at $\lambda = 1529.4\,\mathrm{nm}$ and $1546.6\,\mathrm{nm}$ shown in Figs. 4(b) and 4(d). The largest TMOKE intensities can be attributed to the minimized denominator in Eq. (3) at the cut-off condition. Compared with the previous experimental studies, which have reported that the TMOKE intensities equivalent to the $\Delta R/R$ were about 0.1%–10%,[10,11,18,28–33] our nearly 100% TMOKE intensity is a result of the perfect momentum matching which can be designed as long as the DDFM system finds the cut-off condition and reinforces large utility of this system.

In summary, we have demonstrated the cut-off condition of SPPs' waveguide mode in the DDFM structure, its wavelength tunability, its controllability on magnetization reversal, and a large enhancement of the TMOKE there. We first designed the $Al_2O_3/SiO_2/Fe$ structures with the cut-off condition around the optical telecommunication wavelengths ($\lambda = 1.3\,\mu$m and $1.55\,\mu$m) according to the cut-off of a waveguide mode based on the Effective index theory, and then we prepared samples and investigated them with the ATR experiment in the Otto configuration. Our samples showed that the absolute reflectance minimum appeared at the designed cut-off wavelength, which in turn was able to be controlled and switched by the application of a moderate external magnetic field. We also obtained a strong TMOKE enhancement just at the cut-off condition. Our straightforward experiment without minute waveguides fabrication will help develop further studies on the long-range propagation of SPPs on a ferromagnetic metal with variable attenuation capability on magnetization reversal, which might open up innovative routes for plasmonic functional devices.

A.C. and G.A. would like to acknowledge funding from the Spanish Ministry of Economy and Competitivity under Grant No. MAT2014-58860-P. H.S. would like to acknowledge Grant-in-Aid for Scientific Research (Nos. 24656010 and 15K13942) from the Ministry of Education, Culture, Sports, Science, and Technology, Japan.

[1]G. Armelles, A. Cebollada, A. García-Martín, and M. U. González, Adv. Opt. Mater. **1**, 10 (2013).
[2]P. Bertrand, C. Hermann, G. Lampel, J. Peretti, and V. I. Safarov, Phys. Rev. B **64**, 235421 (2001).
[3]H. Uchida, Y. Masuda, R. Fujikawa, A. V. Baryshev, and M. Inoue, J. Magn. Magn. Mater. **321**, 843 (2009).
[4]H. Uchida, Y. Mizutani, Y. Nakai, A. A. Fedyanin, and M. Inoue, J. Phys. D **44**, 064014 (2011).
[5]J. B. González-Díaz, A. García-Martín, J. M. García-Martín, A. Cebollada, G. Armelles, B. Sepúlveda, Y. Alaverdyan, and M. Käll, Small **4**, 202 (2008).
[6]D. Meneses-Rodríguez, E. Ferreiro-Vila, P. Prieto, J. Anguita, M. U. González, J. M. García-Martín, A. Cebollada, A. García-Martín, and G. Armelles, Small **7**, 3317 (2011).
[7]J. C. Banthí, D. Meneses-Rodríguez, F. García, M. U. González, A. García-Martín, and G. Armelles, Adv. Mater. **24**, OP36 (2012).
[8]H. Y. Feng, F. Luo, D. Meneses-Rodríguez, G. Armelles, and A. Cebollada, Appl. Phys. Lett. **106**, 083105 (2015).
[9]H. Y. Feng, F. Luo, R. Kekesi, D. Granados, D. Meneses-Rodríguez, J. M. García, A. García-Martín, G. Armelles, and A. Cebollada, Adv. Opt. Mater. **2**, 612 (2014).
[10]J. B. González-Díaz, A. García-Martín, G. Armelles, J. M. García-Martín, C. Clavero, A. Cebollada, R. A. Lukaszew, J. R. Skuza, D. P. Kumah, and R. Clarke, Phys. Rev. B **76**, 153402 (2007).
[11]B. Caballero, A. García-Martín, and J. C. Cuevas, Phys. Rev. B **85**, 245103 (2012).
[12]V. I. Belotelov, D. A. Bykov, L. L. Doskolovich, A. N. Kalish, and A. K. Zvezdin, Sov. Phys. JETP **110**, 816 (2010).
[13]V. V. Temnov, G. Armelles, U. Woggon, D. Guzatov, A. Cebollada, A. García-Martín, J. M. García-Martín, T. Thomay, A. Leitenstorfer, and R. Bratschitsch, Nat. Photonics **4**, 107 (2010).
[14]B. Sepúlveda, L. M. Lechuga, and G. Armelles, J. Lightwave Technol. **24**, 945 (2006).
[15]J. B. Khurgin, Appl. Phys. Lett. **89**, 251115 (2006).
[16]V. Zayets, H. Saito, S. Yuasa, and K. Ando, J. Appl. Phys. **111**, 023103 (2012).
[17]V. Zayets, H. Saito, K. Ando, and S. Yuasa, Materials **5**, 857 (2012).
[18]B. Sepúlveda, A. Calle, L. M. Lechuga, and G. Armelles, Opt. Lett. **31**, 1085 (2006).
[19]Y. Shoji and T. Mizumoto, Sci. Technol. Adv. Mater. **15**, 014602 (2014).
[20]E. Kretschmann and H. Raether, Z. Naturforsch. A **23**, 2135 (1968).
[21]A. Otto, Z. Phys. **216**, 398 (1968).
[22]V. Zayets, H. Saito, K. Ando, and S. Yuasa, Opt. Express **23**, 12834 (2015).
[23]T. Kaihara, T. Ando, H. Shimizu, V. Zayets, H. Saito, K. Ando, and S. Yuasa, Opt. Express **23**, 11537 (2015).
[24]A. Yariv and P. Yeh, *Photonics: Optical Electronics in Modern Communications*, 6th ed. (Oxford University Press, New York, 2007), p. 137, 199.
[25]A. Berger and M. R. Pufall, Appl. Phys. Lett. **71**, 965 (1997).
[26]G. Neuber, R. Rauer, J. Kunze, T. Korn, C. Pels, G. Meier, U. Merkt, J. Bäckström, and M. Rübhausen, Appl. Phys. Lett. **83**, 4509 (2003).
[27]R. Rauer, G. Neuber, J. Kunze, J. Bäckström, and M. Rübhausen, Rev. Sci. Instrum. **76**, 023910 (2005).
[28]D. Regatos, D. Fariña, A. Calle, A. Cebollada, B. Sepúlveda, G. Armelles, and L. M. Lechuga, J. Appl. Phys. **108**, 054502 (2010).
[29]V. I. Belotelov, I. A. Akimov, M. Pohl, V. A. Kotov, S. Kasture, A. S. Vengurlekar, A. V. Gopal, D. R. Yakovlev, A. K. Zvezdin, and M. Bayer, Nat. Nanotechnol. **6**, 370 (2011).
[30]L. E. Kreilkamp, V. I. Belotelov, J. Y. Chin, S. Neutzner, D. Dregely, T. Wehlus, I. A. Akimov, M. Bayer, B. Stritzker, and H. Giessen, Phys. Rev. X **3**, 041019 (2013).
[31]M. Pohl, L. E. Kreilkamp, V. I. Belotelov, I. A. Akimov, A. N. Kalish, N. E. Khokhlov, V. J. Yallapragada, A. V. Gopal, M. Nur-E-Alam, M. Vasiliev, D. R. Yakovlev, K. Alameh, A. K. Zvezdin, and M. Bayer, New J. Phys. **15**, 075024 (2013).
[32]N. Kostylev, I. S. Maksymov, A. O. Adeyeye, S. Samarin, M. Kostylev, and J. F. Williams, Appl. Phys. Lett. **102**, 121907 (2013).
[33]H.-T. Huang, P.-J. Chen, T.-R. Ger, Y.-J. Chi, C.-W. Huang, K.-T. Liao, J.-Y. Lai, J.-Y. Chen, W.-Y. Peng, Q. Zhang, T.-F. Hsieh, W.-J. Sheu, and Z.-H. Wei, IEEE Trans. Magn. **50**, 1001604 (2014).